J. Plasma Physics (1998), *vol.* 60, *part* 4, *pp.* 787–810. Printed in the United Kingdom

Photoabsorption by an ion immersed in a plasma at any temperature

K. ISHIKAWA,[1] B. U. FELDERHOF,[1] T. BLENSKI[2] and B. CICHOCKI[3]

[1]Institut für Theoretische Physik A, RWTH Aachen, Templergraben 55, 52056 Aachen, Germany

[2]DSM/DRECAM/SPAM, CEA Saclay, F 91191 Gif-sur-Yvette Cedex, France

[3]Institute of Theoretical Physics, Warsaw University, Hoza 69, 00-618 Warsaw, Poland

(Received 2 February 1998 and in revised form 23 June 1998)

The photoabsorption cross-section of an ion immersed in a plasma is studied on the basis of the Thomas–Fermi approximation for the equilibrium electron distribution and Bloch's classical hydrodynamic model for collective motion of the electrons. The frequency-dependent cross-section scales with the nuclear charge, and depends strongly on the plasma density and temperature. An approximation of the frequency dependence is constructed with the aid of sum rules and Padé approximants.

1. Introduction

The theory of photoabsorption by ions in a plasma is relevant for the calculation of plasma opacity – a crucial concept in inertial confinement fusion and stellar structure. The early history of opacity calculations is reviewed in the monograph by Armstrong and Nicholls (1972). Existing opacity codes (Goldberg *et al.* 1986; Bar-Shalom *et al.* 1989; Abdallah and Clark 1991; Rogers and Iglesias 1992; Keady *et al.* 1993; Blenski *et al.* 1997) use the main features of the model proposed by Mayer (1949). In this model the electrons are divided into two categories: atomically bound and free electrons. All intermediate bound states, for example quasimolecular states, are neglected, on the basis of their small statistical weight. In Mayer's model, and subsequently probably in all existing opacity codes, the photoabsorption cross-section is divided into bound–bound (b–b), bound-free (b–f) and free-free (f–f) contributions. In the model the interaction between bound and free electrons is neglected, but in existing opacity codes part of the dynamic correlation between bound and free electrons is accounted for as line broadening. The modern opacity codes have reached a high level of sophistication in the treatment of bound–bound transitions. Term structure is taken into account either by statistical methods (Bar-Shalom *et al.* 1989; Blenski *et al.* 1997) or by detailed term accounting (Goldberg et al. 1986; Abdallah & Clark 1991; Rogers & Iglesias 1992; Keady *et al.* 1993). However, the division into b–b, b–f and f–f transitions is still used in the codes.

Probably one of the reasons that present-day opacity codes focus their attention on the b–b and b–f transitions is the fact that up to now all direct opacity measurements (Davidson *et al.* 1988; Foster *et al.* 1991; Perry *et al.* 1991; Da Silva *et al.*

1992), have been performed in plasmas of relatively low density (0.05 g cm^{-3} at most). This is because of the hydrodynamic expansion scenario of the sandwich-type targets in present-day laser–plasma experiments. The neglect of correlation between bound and free electrons seems to be justified when the plasma density is small compared with solid density, and when one is interested in photoabsorption at relatively high frequencies. There are two reasons for this. First, for small plasma density, of the order of one percent of solid density, the plasma frequency is small (less than 1 eV). Secondly, the total charge of the free electrons contained in the ionic core, where the bound electrons are localized, is negligible. Thus a pure atomic physics approach dealing with free ions, supplemented by thermal statistics for all species as given for example by Saha equilibrium theory, seems to be sufficient to interpret the spectral data from present-day opacity measurements, similar to those presented in Davidson *et al.* (1988), Foster *et al.* (1991), Perry *et al.* (1991) and Da Silva *et al.* (1992).

It was shown by Zangwill and Soven (1980) and Zangwill and Liberman (1984), in a calculation of the photoabsorption of rare-gas atoms based on the local density functional method, that channel mixing between the *b–b* and *b–f* transitions is very important (Mahan and Subbaswamy 1990). There have been attempts to apply the method of Zangwill and Soven (1980) to ions in a plasma (Grimaldi *et al.* 1985; Perrot and Dharma-wardana 1993). However, in this work the interaction with free–free transitions was neglected without justification, even though bound and free electrons should be treated on equal footing.

In fusion experiments with high-energy lasers of the next generation, it will be possible to achieve one-tenth of solid density at temperatures of a few tens of eV for an aluminum sandwich target (Lee *et al.* 1995). A complete treatment of photoabsorption in dense plasmas under such conditions is difficult. Besides the free–free transitions due to collisions with atomic centers, collective phenomena also become important (Blenski and Cichocki 1992, 1994). Channel mixing between *b–b*, *b–f* and *f–f* transitions is known to be quite important in metals (Zaremba and Sturm 1991; Sturm *et al.* 1990). Mayer's (1949) model is probably not a good starting point for the calculation of photoabsorption in dense plasmas. In previous work (Blenski and Cichocki 1992, 1994; Felderhof *et al.* 1995*a*, *b*, *c*) we have proposed that a cluster expansion, allowing a decomposition of the many-ion problem into a superposition of few-ion problems, provides the correct theoretical approach. However, a full quantum mechanical treatment of photoabsorption, even for a single ion immersed in a plasma, is a very demanding task. Therefore in the present study we use a simple semiclassical approach in order to get qualitative insight. The calculation is based on the Thomas–Fermi model combined with classical hydrodynamics, as used by Bloch (1933) in a calculation of the stopping power of atoms. The same model was used by Ball *et al.* (1973) for the calculation of photoabsorption by an atom. The model takes account of collective motion, but single electron processes are not included. Thus we cannot expect detailed agreement with opacity measurements. Nonetheless, we believe that the calculation reveals important qualitative features.

In the following we extend the work of Ball *et al.* (1973) to an ion immersed in a plasma at any temperature. We use an ion correlation model in which the other ions in the plasma appear only in their average effect on the equilibrium distribution of electrons (Perrot 1982; Cauble *et al.* 1984; Crowley 1990). Rather than calculate the ion correlation function, we assume it to be known. Specifically, we assume that the equilibrium distribution of electrons can be calculated in the Thomas–Fermi

approximation, with the nuclear point charge of the selected ion at fixed position and the remaining ions smeared out into a uniform neutralizing background. The calculation can be modified without difficulty to a different ion correlation function and corresponding radial electron density profile.

Within the framework of Bloch's hydrodynamic model, the dielectric linear response of the entire plasma can be analysed by the method of cluster expansion (Felderhof *et al.* 1995*a*; Ishikawa and Felderhof 1998). The analysis shows how to incorporate the response calculated for the ion correlation model into the dielectric function of the plasma. In the ion correlation model the plasma is uniform at large distances from the central ion. In an incident oscillating electric field the charge distribution of the ion vibrates and generates outgoing plasma waves. We use an electrostatic dipole approximation. Photoabsorption occurs because incident wave energy is converted into the energy of longitudinal plasma waves. We find for our model that the frequency-dependent photoabsorption cross-section scales with the nuclear charge and depends strongly on plasma density and temperature.

Our method of calculation of the frequency-dependent photoabsorption cross-section differs from that of Ball *et al.* (1973). It was developed for a general radial electron density profile (Felderhof *et al.* 1995*b*), and applied to the explicit calculation of photoabsorption for a model ion with a square-well profile (Felderhof *et al.* 1995*c*). The method is rather more straightforward than that of Ball *et al.* (1973).

The equilibrium electron density profile can be decomposed into contributions from bound and free electrons. We determine the degree of ionization as a function of plasma density and temperature. In the calculation of the photoabsorption cross-section we make no attempt to separate into contributions from bound and free electrons. Since only the total cross-section counts, not much would be gained from such a decomposition. It would be of interest to adorn the model with an ion core polarizability with discrete resonances, in the manner proposed by Sturm and Zaremba (1991) and Sturm *et al.* (1990) for metals. This would provide a qualitative description of the mixing of single-particle and collective effects.

2. Thomas–Fermi model for an ion in a plasma

We consider an electron–ion plasma in a volume V with the ions treated as point charges Ze located at $\mathbf{R}_1, \ldots, \mathbf{R}_N$ and with electrons described collectively as a fluid with local density $n(\mathbf{r}, t)$ and flow velocity $\mathbf{v}(\mathbf{r}, t)$. The electron density and flow velocity are assumed to satisfy the hydrodynamic equations (Bloch 1933)

$$\frac{\partial n}{\partial t} + \boldsymbol{\nabla} \cdot (n\mathbf{v}) = 0, \tag{2.1a}$$

$$nm\frac{d\boldsymbol{v}}{dt} = -\boldsymbol{\nabla} p + ne\boldsymbol{\nabla}\phi, \tag{2.1b}$$

where m is the electron mass, $-e$ is the electron charge and $d/dt = \partial/\partial t + \mathbf{v} \cdot \boldsymbol{\nabla}$ is the substantial derivative. The pressure p is assumed to be related to local number density n by the equation of state $p = p(n, T)$ for an ideal Fermi gas at temperature T. The electrostatic potential $\phi(\mathbf{r}, t)$ is governed by Poisson's equation

$$\nabla^2\phi = 4\pi ne - 4\pi\rho_f - 4\pi\rho_{\mathrm{ex}}, \tag{2.2}$$

where

$$\rho_f(\mathbf{r}) = Ze \sum_{j=1}^{N} \delta(\mathbf{r} - \mathbf{R}_j) \tag{2.3}$$

is the charge density of the fixed ions and $\rho_{\rm ex}(\mathbf{r}, t)$ is the external charge density. For $\rho_{\rm ex} = 0$, the equations are satisfied by equilibrium density $n_0(\mathbf{r}; \mathbf{R}_1, \ldots, \mathbf{R}_N)$ and flow velocity $\mathbf{v}_0 = 0$. For the equation of state of an ideal Fermi gas, the equilibrium density $n_0(\mathbf{r}; \mathbf{X})$ is the Thomas–Fermi solution for the given configuration $\mathbf{X} = (\mathbf{R}_1, \ldots, \mathbf{R}_N)$ of ion centres (Landau and Lifshitz 1965; Englert 1988). The local chemical potential μ_0 and the electrostatic potential ϕ_0 combine as

$$\mu_0(\mathbf{r}; \mathbf{X}) - e\phi_0(\mathbf{r}; \mathbf{X}) = \text{const}, \tag{2.4}$$

with the constant value of the electrochemical potential chosen in such a way that the whole system is neutral.

The linear response of the system to an external charge density $\rho_{\rm ex}(\mathbf{r}, t)$ with corresponding potential $\phi_{\rm ex}(\mathbf{r}, t)$ can be handled by the methods of multiple scattering and cluster expansion (Felderhof *et al.* 1995*a*; Ishikawa and Felderhof 1998*a*). To lowest order in the cluster expansion, the system is approximated as a one-component plasma. In equilibrium, this has uniform electron density $n_0^{(0)} = Z_0\, n_i$ and a fixed uniform background of charge density $Z_0\, n_i e$. Later we shall determine the effective charge number Z_0 self-consistently by identifying $n_0^{(0)}$ with the number density of free electrons. Some of the electrons are bound to the nuclei and do not contribute to the response of the one-component plasma. The equilibrium electrostatic potential ϕ_0 of the one-component plasma vanishes, and the chemical potential $\mu_0^{(0)}$ of the free electrons is related to $n_0^{(0)}$ by the equation of state for an ideal Fermi gas. In the thermodynamic limit $N \to \infty$, $V \to \infty$ at constant $n_i = N/V$ the dielectric response functions of this electron−0−ion system are easily calculated from the linearized hydrodynamic equations.

To first order in the cluster expansion, one considers an electron–1-ion system characterized by an equilibrium density profile $\bar{n}_0(\mathbf{r}; \mathbf{R}_1)$ corresponding to a mean density of electrons with a single nucleus of charge Ze centred at $\mathbf{R}_1$. In addition, one needs the profile $\bar{\vartheta}_0(\mathbf{r}; \mathbf{R}_1)$ corresponding to a mean local derivative $(\partial\mu/\partial n)_{n_0}$ of the chemical potential with respect to density. At large distances from $\mathbf{R}_1$ the density $\bar{n}_0(\mathbf{r}; \mathbf{R}_1)$ tends to the uniform free-electron value $n_0^{(0)}$, and the profile $\bar{\vartheta}_0(\mathbf{r}; \mathbf{R}_1)$ tends to the corresponding value $\vartheta_0^{(0)}$. The cluster expansion shows how to incorporate the response of the electron–1-ion system to an applied field into an approximation to the response of the plasma with N ions.

The calculation of the profiles $\bar{n}_0(\mathbf{r}; \mathbf{R}_1)$ and $\bar{\vartheta}_0(\mathbf{r}; \mathbf{R}_1)$ from the microscopic equilibrium functions $n_0(\mathbf{r}; \mathbf{X})$ and $\vartheta_0(\mathbf{r}; \mathbf{X})$ is in itself a non-trivial problem. In the following we circumvent this problem and simply postulate a prescription for finding approximate profiles from Thomas–Fermi theory. We describe the prescription separately for zero temperature and for temperature $T > 0$. At zero temperature, the Fermi–Dirac theory of the ideal gas shows that density $\bar{n}_0$ and chemical potential $\bar{\mu}_0$ are related by

$$\bar{\mu}_0 = \frac{h^2}{2m} \left(\frac{3\bar{n}_0}{8\pi}\right)^{2/3}, \tag{2.5}$$

where h is Planck's constant. Without loss of generality, we place the centre $\mathbf{R}_1$

at the origin. In Thomas–Fermi theory (Landau and Lifshitz 1965; Englert 1988), (2.5) is taken to be valid locally in the form

$$\bar{\mu}_0(r) = \mu_0^{(0)} + e\phi_0(r) = \frac{h^2}{2m}\left(\frac{3}{8\pi}\bar{n}_0(r)\right)^{2/3} \tag{2.6}$$

with the potential ϕ_0 determined from Poisson's equation

$$\nabla^2\phi_0 = 4\pi e[\bar{n}_0(r) - n_0^{(0)}] - 4\pi Ze\delta(\mathbf{r}). \tag{2.7}$$

The last two equations must be solved self-consistently, with the condition that $\phi_0(r)$ tends to zero at infinity. The derivative $\vartheta_0 = (\partial\mu/\partial n)_{n_0}$ leads to the corresponding profile

$$\bar{\vartheta}_0(r) = \frac{2}{3}\,\frac{\bar{\mu}_0(r)}{\bar{n}_0(r)}. \tag{2.8}$$

Introducing the dimensionless distance x by

$$r = Z^{-1/3}\,ba_0x, \qquad b = \tfrac{1}{2}\left(\tfrac{3\pi}{4}\right)^{2/3}, \tag{2.9}$$

where $a_0 = \hbar^2/me^2$ is the Bohr radius, and the function $\chi(x)$ by

$$\phi_0(r) = \frac{Ze}{r}\,\chi(x), \tag{2.10}$$

we find for $\chi(x)$ the radial equation

$$\frac{d^2\chi}{dx^2} = \frac{1}{x^{1/2}}\,\{[\chi(x) + C\,x]^{3/2} - C^{3/2}\,x^{3/2}\}, \tag{2.11}$$

with the constant

$$C = Z^{-4/3}(4\pi b^3\,n_0^{(0)}\,a_0^3)^{2/3}. \tag{2.12}$$

The boundary conditions are

$$\chi(0) = 1, \qquad \lim_{x\to\infty}\chi(x) = 0. \tag{2.13}$$

The radial equation (2.11) generalizes the corresponding equation for an atom in vacuum (Landau and Lifshitz 1965), for which $C = 0$, to the case of an ion in a plasma. The density profile $\bar{n}_0(r)$ in (2.6) can be expressed as

$$\bar{n}_0(r) = \frac{Z^2}{b^3a_0^3}\,\hat{n}_0(x), \tag{2.14}$$

with the dimensionless profile

$$\hat{n}_0(x) = \frac{1}{4\pi}\left[\frac{\chi(x)}{x} + C\right]^{3/2}. \tag{2.15}$$

The profile $\hat{n}_0(x)$ depends on Z only via the parameter C.

For temperature $T > 0$, the electron equilibrium distribution in $(\mathbf{r},\mathbf{p})$ space is

$$f(\mathbf{r},\mathbf{p}) = \frac{2}{h^3}\left\{\exp\left[\beta\left(\frac{p^2}{2m} - e\phi_0(r) - \mu_0^{(0)}\right)\right] + 1\right\}^{-1}, \tag{2.16}$$

where $\beta = 1/k_BT$. By integration over momentum $\mathbf{p}$, one finds for the local electron density

$$\overline{n_0}(r) = \int f(\mathbf{r},\mathbf{p})\,d\mathbf{p} = \frac{4}{\pi^{1/2}}\,\lambda_{dB}^{-3}\,F_{1/2}\left(\frac{\mu_0^{(0)} + e\phi_0(r)}{k_BT}\right) \tag{2.17}$$

with de Broglie wavelength $\lambda_{dB} = h(2\pi m\, k_B T)^{-1/2}$ and Fermi–Dirac integral (Cody and Thacher 1967; Antia 1993)

$$F_{1/2}(z) = \int_0^\infty \frac{y^{1/2}}{\exp(y-z)+1}\, dy. \tag{2.18}$$

The constant $\mu_0^{(0)}$ is related to the asymptotic density $n_0^{(0)}$ by

$$n_0^{(0)} = \frac{4}{\pi^{1/2}} \lambda_{dB}^{-3}\, F_{1/2}\left(\frac{\mu_0^{(0)}}{k_B T}\right). \tag{2.19}$$

The electrostatic potential $\phi_0(r)$ is given by Poisson's equation (2.7). The dimensionless function $\chi(x)$, defined by (2.10), satisfies the radial equation

$$\frac{d^2\chi}{dx^2} = \tfrac{3}{2}\gamma^{-3/2}\, x[F_{1/2}(\alpha_0(x)) - F_{1/2}(\alpha_0^{(0)})], \tag{2.20}$$

with coefficient

$$\gamma = Z^{4/3}\, \frac{e^2}{k_B T b a_0}, \tag{2.21}$$

and with the local reduced chemical potential

$$\alpha_0(x) = \alpha_0^{(0)} + \gamma \frac{\chi(x)}{x}, \tag{2.22}$$

which takes the value

$$\alpha_0^{(0)} = \frac{\mu_0^{(0)}}{k_B T} \tag{2.23}$$

at infinity. The boundary conditions on $\chi(x)$ are the same as in (2.13). It is easily shown that the solution of (2.20) tends to the solution of (2.11) in the limit of zero temperature. It follows from (2.19) that the reduced chemical potential $\alpha_0^{(0)}$ is determined by the product $n_0^{(0)}\lambda_{dB}^3$.

The profile $\bar{n}_0(r)$ follows from the solution of (2.20) via (2.10) and (2.17). From (2.17), one finds for the profile $\bar{\vartheta}_0(r)$

$$\bar{\vartheta}_0(r) = \frac{\pi^{1/2}}{4} \frac{\lambda_{dB}^3\, k_B T}{F'_{1/2}(\alpha_0(x))}. \tag{2.24}$$

It is convenient to scale temperature and chemical potential as

$$k_B T = \frac{Z^{4/3} e^2}{b a_0} \hat{T}, \tag{2.25a}$$

$$\mu_0^{(0)} = \frac{Z^{4/3} e^2}{b a_0} \hat{\mu}_0^{(0)}. \tag{2.25b}$$

Then the profile $\bar{\vartheta}_0(r)$ scales as

$$\bar{\vartheta}_0(r) = Z^{-2/3}\, e^2\, b^2\, a_0^2\ \hat{\vartheta}_0(x), \tag{2.26}$$

with

$$\hat{\vartheta}_0(x) = \frac{8\pi}{3} \frac{\gamma^{1/2}}{F'_{1/2}\,(\alpha_0(x))}. \tag{2.27}$$

The density profile $\bar{n}_0(r)$ can be written as in (2.10), with

$$\hat{n}_0(x) = \frac{3}{8\pi}\,\gamma^{-3/2}\,F_{1/2}\,(\alpha_0(x)). \tag{2.28}$$

The reduced profiles $\hat{n}_0(x)$ and $\hat{\vartheta}_0(x)$ depend on the parameters $\alpha_0^{(0)}$ and $\hat{T} = \gamma^{-1}$, but not explicitly on Z. They can be found by numerical integration of the differential equation (2.20).

3. Electron density profile

In this section we study the equilibrium electron density profile $\bar{n}_0(r)$ in some more detail. The Fermi–Dirac integral $F_{1/2}(z)$, defined in (2.18), behaves for large z as (Landau and Lifshitz 1968)

$$F_{1/2}(z) = \tfrac{2}{3}\,z^{3/2} + \frac{\pi^2}{12 z^{1/2}} + O(z^{-5/2}). \tag{3.1}$$

At small distance, the potential $\phi_0(r)$ diverges as Ze/r, so that we find from (2.28)

$$\hat{n}_0(x) \sim \frac{1}{4\pi x^{3/2}} \qquad \text{as} \qquad x \to 0, \tag{3.2}$$

independent of $\alpha_0^{(0)}$ and γ. The strong attraction by the nucleus causes singular behaviour of the electron density. At large distance from the nucleus, the potential is screened. By expansion in (2.20), one finds

$$\chi(x) \sim \chi_\infty\, e^{-\hat{\kappa} x} \qquad \text{as} \qquad x \to \infty, \tag{3.3}$$

with $\hat{\kappa}$ given by

$$\hat{\kappa}^2 = \frac{4\pi}{\hat{\vartheta}_0^{(0)}}. \tag{3.4}$$

Correspondingly, the electrostatic potential behaves as

$$\phi_0(r) \sim \chi_\infty\, Ze\,\frac{\exp(-\kappa r)}{r} \qquad \text{as} \qquad r \to \infty, \tag{3.5}$$

with inverse screening length κ given by

$$\kappa^2 = \frac{4\pi e^2}{\vartheta_0^{(0)}}. \tag{3.6}$$

The reduction factor χ_∞ must be determined numerically from (2.20). From (2.17), we find for the density profile

$$\bar{n}_0(r) \sim n_0^{(0)} + \chi_\infty\,\frac{Z\kappa^2}{4\pi}\,\frac{\exp(-\kappa r)}{r} \qquad \text{as} \qquad r \to \infty. \tag{3.7}$$

The dimensionless profile $\hat{n}_0(x)$ behaves as

$$\hat{n}_0(x) \sim \hat{n}_0^{(0)} + \chi_\infty \frac{\hat{\kappa}^2}{4\pi}\frac{\exp(-\hat{\kappa} x)}{x} \qquad \text{as} \qquad x \to \infty. \tag{3.8}$$

In the low-temperature limit, κ is the inverse of the Thomas–Fermi screening length,

$$\kappa^2 = \frac{3}{b a_0}\left(\frac{\pi n_0^{(0)}}{2}\right)^{1/3} \qquad (T = 0). \tag{3.9}$$

At high temperature, κ^2 is given by the Debye–Hückel expression

$$\kappa^2 = \frac{4\pi n_0^{(0)} e^2}{k_B T} \qquad (T \to \infty). \tag{3.10}$$

The screening of the potential shows that the integral of the density profile is

$$\int_0^\infty [\overline{n_0}(r) - n_0^{(0)}] r^2 \, dr = \frac{Z}{4\pi}. \tag{3.11}$$

Correspondingly,

$$\int_0^\infty [\hat{n}_0(x) - \hat{n}_0^{(0)}] x^2 \, dx = \frac{1}{4\pi}. \tag{3.12}$$

Electrons that at distance r have kinetic energy $p^2/2m$ less than $e\phi_0(r)$ are bound. Hence we can write the density profile as a sum of bound- and free-electron contributions:

$$\bar{n}_0(r) = \bar{n}_b(r) + \bar{n}_f(r), \tag{3.13}$$

with $\bar{n}_b(r)$ given by

$$\bar{n}_b(r) = \frac{4}{\pi^{1/2}} \lambda_{dB}^{-3} F_{1/2}\left(\frac{\mu_0^{(0)} + e\phi_0(r)}{k_B T}, \, \frac{e\phi_0(r)}{k_B T} \right), \tag{3.14}$$

with $F_{1/2}(z, y_0)$ defined by

$$F_{1/2}(z, y_0) = \int_0^{y_0} \frac{y^{1/2}}{\exp(y - z) + 1} \, dy. \tag{3.15}$$

The degree of ionization

$$I_f = \frac{Z_f}{Z} \tag{3.16}$$

follows from

$$\int_0^\infty [\bar{n}_f(r) - n_0^{(0)}] r^2 \, dr = \frac{Z_f}{4\pi}. \tag{3.17}$$

One can now identify $Z_0 = Z_f$. We recall that $Z_0 \, n_i e$ is the charge density of the neutralizing background. If the ion density n_i is prescribed then the relation $n_0^{(0)} = Z_f \, n_i$ provides a self-consistent equation from which $n_0^{(0)}$ can be determined as a function of Z, n_i and temperature T. Conversely, if the free-electron density is given then the ion density can be calculated as $n_i = n_0^{(0)}/Z_f$. Corresponding to (3.14), we define the dimensionless profile

$$\hat{n}_b(x) = \frac{3}{8\pi} \gamma^{-3/2} \, F_{1/2}(\alpha_0(x), \gamma \, \chi(x)). \tag{3.18}$$

The degree of ionization as a function of $\alpha_0^{(0)}$ and γ is

$$I_f = 4\pi \int_0^\infty [\hat{n}_f(x) - \hat{n}_0^{(0)}] x^2 \, dx. \tag{3.19}$$

In Fig. 1 we plot I_f as a function of reduced temperature $\hat{T}$ for several asymptotic electron densities $\hat{n}_0^{(0)}$. It is somewhat surprising that the degree of ionization first decreases with temperature before increasing monotonically at higher temperature. In Fig. 2 we plot I_f as a function of density $\hat{n}_0^{(0)}$ for several values of $\hat{T}$. The degree of ionization first decreases with density before increasing monotonically

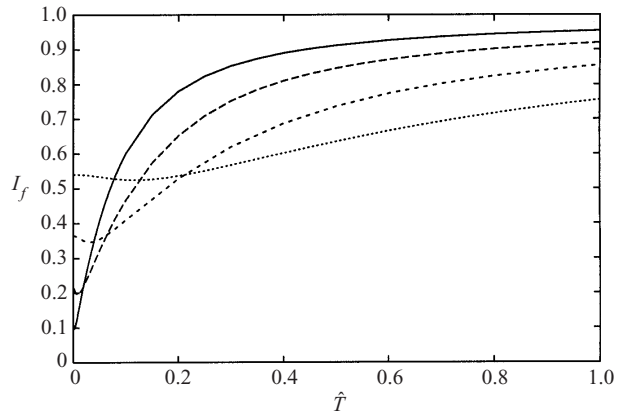

Figure 1. Degree of ionization I_f, as given by (3.19), as a function of reduced temperature $\hat{T}$ for reduced density $\hat{n}_0^{(0)} = 10^{-5}$ (solid line), 10^{-4} (long dashes), 10^{-3} (short dashes) and 10^{-2} (dotted line).

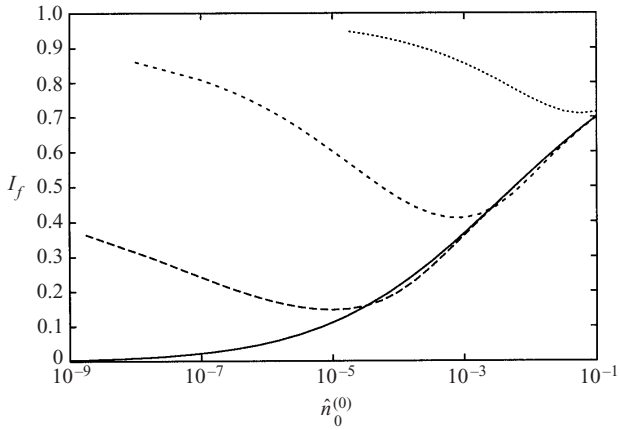

Figure 2. Degree of ionization I_f as a function of reduced density $\hat{n}_0^{(0)}$ for reduced temperature $\hat{T} = 0$ (solid line), 0.01 (long dashes), 0.1 (short dashes), and 1 (dotted line).

at higher density. Thus the degree of ionization I_f depends in a complicated way on asymptotic electron density $\hat{n}_0^{(0)}$ and temperature $\hat{T}$, owing to the interplay of the change of shape of the self-consistent electrostatic potential $\phi_0(r)$ and the occupation of levels in this potential. In Fig. 3 we plot the profile $\hat{n}_0(x)$ as a function of dimensionless distance x for density $\hat{n}_0^{(0)} = 10^{-5}$ and various reduced temperatures $\hat{T}$. In Fig. 4 we present similar plots for $\hat{n}_0^{(0)} = 0.001$. It is evident that for fixed asymptotic density the electron density in the intermediate range decreases with temperature due to ionization. In Fig. 5 we plot the function $\chi(x)\exp(\hat{\kappa}x)$ as a function of x for density $\hat{n}_0^{(0)} = 10^{-5}$ and various reduced temperatures $\hat{T}$. The function starts at unity for $x = 0$ and tends to the reduction factor χ_∞ for large x. The reduction factor χ_∞ first decreases and then increases with temperature. In Fig. 6 we present similar plots for $\hat{n}_0^{(0)} = 0.001$.

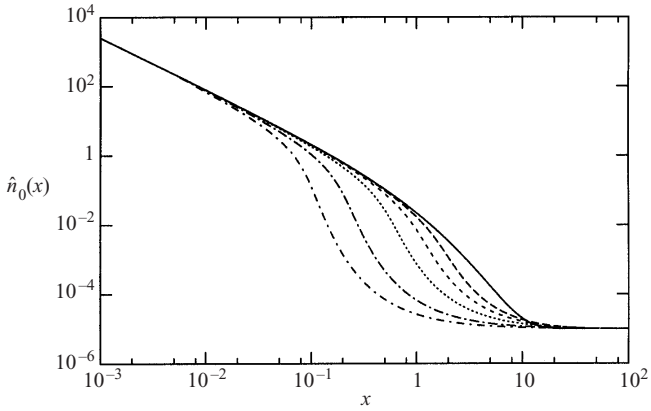

Figure 3. Equilibrium electron density profile $\hat{n}_0(x)$ as a function of dimensionless distance x for asymptotic density $\hat{n}_0^{(0)} = 10^{-5}$ and reduced temperature $\hat{T} = 0$ (solid line), 0.05 (long dashes), 0.1 (short dashes), 0.2 (dotted line), 0.5 (long dashes, dots) and 1 (short dashes, dots).

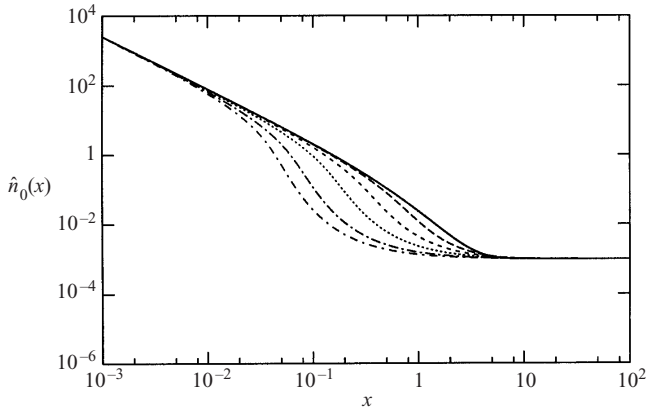

Figure 4. Equilibrium electron density profile $\hat{n}_0(x)$ as a function of dimensionless distance x for asymptotic density $\hat{n}_0^{(0)} = 0.001$ and reduced temperature $\hat{T} = 0$ (solid line), 0.2 (long dashes), 0.5 (short dashes), 1 (dotted line), 2 (long dashes, dots) and 3 (short dashes, dots).

4. Induced dipole moment

In order to calculate the photoabsorption cross-section, one considers the linear response of the electron–1-ion system to a uniform oscillating electric field $\mathbf{E}^{(0)}(t) = \mathbf{E}_\omega^{(0)} \exp(-i\omega t)$. The equations of motion (2.1) are linearized to (Felderhof *et al.* 1995*b*)

$$\frac{\partial n_1}{\partial t} + \boldsymbol{\nabla} \cdot (\bar{n}_0 \mathbf{v}_1) = 0, \tag{4.1a}$$

$$m \frac{\partial \mathbf{v}_1}{\partial t} = -\boldsymbol{\nabla}(\bar{\vartheta}_0 n_1) + e \boldsymbol{\nabla} \phi_1, \tag{4.1b}$$

and Poisson's equation (2.2) becomes

$$\nabla^2 \phi_1 = 4\pi n_1 e, \tag{4.2}$$

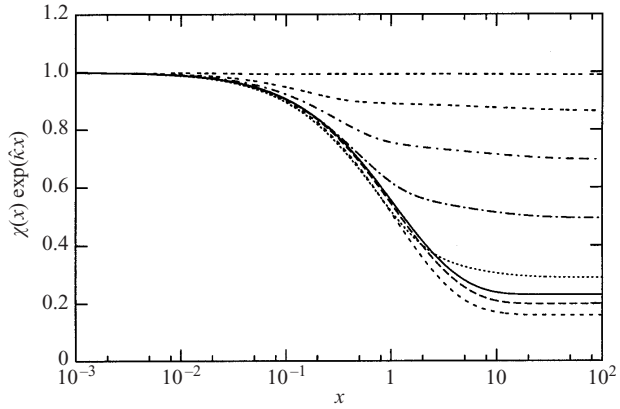

Figure 5. The function $\chi(x)\exp(\hat{\kappa}x)$, as given by (2.20) and (3.4), versus x for density $\hat{n}_0^{(0)} = 10^{-5}$ and reduced temperature $\hat{T} = 0$ (solid line), 0.001 (long dashes), 0.003 (short dashes), 0.02 (dotted line), 0.05 (long dashes, dots), 0.1 (short dashes, dots), 0.2 (double dashes) and 1 (triple dashes).

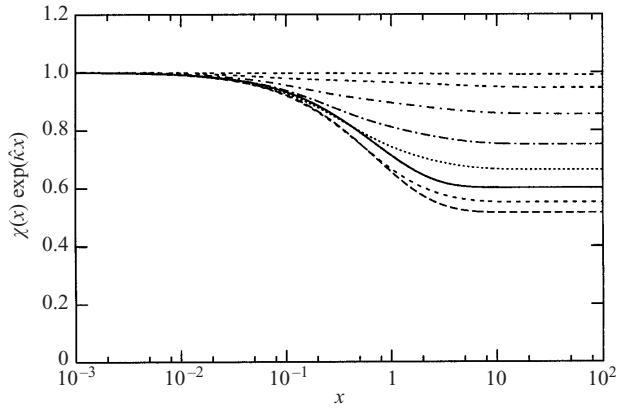

Figure 6. The function $\chi(x)\exp(\hat{\kappa}x)$, as given by (2.20) and (3.4), versus x for density $\hat{n}_0^{(0)} = 0.001$ and reduced temperature $\hat{T} = 0$ (solid line), 0.05 (long dashes), 0.1 (short dashes), 0.2 (dotted line), 0.3 (long dashes, dots), 0.5 (short dashes, dots), 1 (double dashes) and 3 (triple dashes).

since $\rho_{\rm ex}$ vanishes for a uniform applied field. The velocity field $\mathbf{v}_1(\mathbf{r}, t)$ can be derived from a streaming potential, $\mathbf{v}_1 = \boldsymbol{\nabla} S_1$, with

$$m\frac{\partial S_1}{\partial t} = -\bar{\vartheta}_0 n_1 + e\phi_1. \tag{4.3}$$

We put

$$n_1(\mathbf{r}, t) = n_\omega(\mathbf{r})\exp(-i\omega t), \tag{4.4a}$$

$$\phi(\mathbf{r}, t) = \phi_\omega(\mathbf{r})\exp(-i\omega t), \tag{4.4b}$$

$$S_1(\mathbf{r}, t) = S_\omega(\mathbf{r})\exp(-i\omega t), \tag{4.4c}$$

and define

$$\rho_\omega = -en_\omega, \tag{4.5a}$$

$$\sigma_\omega = -\frac{i\omega m}{e} S_\omega. \tag{4.5b}$$

The equations for the Fourier amplitudes ρ_ω, σ_ω and ϕ_ω then read

$$\omega^2 \rho_\omega + \frac{e^2}{m} \boldsymbol{\nabla} \cdot (\bar{n}_0 \boldsymbol{\nabla} \sigma_\omega) = 0, \tag{4.6a}$$

$$\sigma_\omega = \frac{\bar{\vartheta}_0}{e^2} \rho_\omega + \phi_\omega, \tag{4.6b}$$

$$\nabla^2 \phi_\omega = -4\pi \ \rho_\omega. \tag{4.6c}$$

We write

$$\phi_\omega = \phi_\omega^{(0)} + \phi_\omega^{(1)}, \tag{4.7a}$$

$$\sigma_\omega = \sigma_\omega^{(0)} + \sigma_\omega^{(1)}, \tag{4.7b}$$

where $\phi_\omega^{(0)}$ and $\sigma_\omega^{(0)}$ are the values for the electron–0-ion system,

$$\phi_\omega^{(0)}(\mathbf{r}) = -\mathbf{E}_\omega^{(0)} \cdot \mathbf{r}, \tag{4.8a}$$

$$\sigma_\omega^{(0)}(\mathbf{r}) = -\mathbf{E}_\omega^{(0)} \cdot \mathbf{r}. \tag{4.8b}$$

The deviations due to the presence of the ion satisfy

$$\omega^2 \rho_\omega^{(1)} + \frac{e^2}{m} \boldsymbol{\nabla} \cdot (\bar{n}_0 \boldsymbol{\nabla} \, \sigma_\omega^{(1)}) = \frac{e^2}{m} \mathbf{E}_\omega^{(0)} \cdot \boldsymbol{\nabla} \bar{n}_0, \tag{4.9a}$$

$$\sigma_\omega^{(1)} - \frac{\bar{\vartheta}_0}{e^2} \rho_\omega^{(1)} - \phi_\omega^{(1)} = 0, \tag{4.9b}$$

$$\nabla^2 \phi_\omega^{(1)} + 4\pi \, \rho_\omega^{(1)} = 0. \tag{4.9c}$$

For frequencies less than the plasma frequency $\omega_{p0} = (4\pi n_0^{(0)} e^2/m)^{1/2}$, both the streaming potential and the electrostatic potential have dipolar character at large distances, of the form

$$\sigma_\omega^{(1)} = \phi_\omega^{(1)} \sim \frac{\mathbf{p}_\omega^{(1)} \cdot \mathbf{r}}{r^3} \qquad \text{as} \qquad r \to \infty. \tag{4.10}$$

For frequencies higher than the plasma frequency, there is an additional undamped outgoing plasma wave. The extinction cross-section $\sigma_{\text{ext}}(\omega)$ follows from the dipole moment $\mathbf{p}_\omega^{(1)}$.

We choose the z axis in the direction of $\mathbf{E}_\omega^{(0)}$ and use spherical coordinates (r, θ, φ). The fields $\sigma_\omega^{(1)}$, $\phi_\omega^{(1)}$ and $\rho_\omega^{(1)}$ are expressed in terms of dimensionless radial functions $G(x)$, $H(x)$ and $K(x)$ by the definitions

$$\sigma_\omega^{(1)}(\mathbf{r}) = \frac{Z^{4/3} e}{b a_0} \frac{G(x)}{x[\hat{n}_0(x)]^{1/2}} \cos\theta, \tag{4.11a}$$

$$\phi_\omega^{(1)}(\mathbf{r}) = \frac{Z^{4/3} e}{b a_0} \frac{H(x)}{x} \cos\theta, \tag{4.11b}$$

$$\rho_\omega^{(1)}(\mathbf{r}) = \frac{Z^2 e}{b^3 a_0^3} \frac{K(x)}{x} \cos\theta. \tag{4.11c}$$

Upon substitution into (4.9), one then finds the radial equations

$$\frac{d^2 G}{dx^2} - \left(\frac{2}{x^2} + \frac{\hat{n}_0'}{x \hat{n}_0} - \frac{\hat{n}_0'^2}{4\hat{n}_0^2} + \frac{\hat{n}_0''}{2\hat{n}_0} \right) G + b^3 \, \Omega^2 \, \frac{K}{\hat{n}_0^{1/2}} = \hat{E}_\omega^{(0)} \frac{x \hat{n}_0'}{\hat{n}_0{}^{1/2}}, \tag{4.12a}$$

$$\hat{\vartheta}_0 K = \frac{G}{\hat{n}_0{}^{1/2}} - H, \tag{4.12b}$$

$$\frac{d^2H}{dx^2} - \frac{2}{x^2}H + 4\pi K = 0, \tag{4.12c}$$

with the dimensionless frequency $\boldsymbol{\Omega}$ defined by

$$\boldsymbol{\Omega} = \frac{\hbar a_0}{Ze^2}\,\omega, \tag{4.13}$$

and the dimensionless field $\hat{E}_\omega^{(0)}$ defined by

$$\hat{E}_\omega^{(0)} = \frac{b^2 a_0^2}{Z^{5/3}e}\,E_\omega^{(0)}. \tag{4.14}$$

Eliminating K, we can cast (4.12) in the form of a set of coupled differential equations

$$\frac{d^2G}{dx^2} + a_{GG}\,G + a_{GH}H = S, \tag{4.15a}$$

$$\frac{d^2H}{dx^2} + a_{HG}\,G + a_{HH}H = 0, \tag{4.15b}$$

with coefficient functions

$$a_{GG} = -\frac{2}{x^2} - \frac{\hat{n}_0'}{x\hat{n}_0} + \frac{\hat{n}_0'^2}{4\hat{n}_0^2} - \frac{\hat{n}_0''}{2\hat{n}_0} + \frac{b^3\boldsymbol{\Omega}^2}{\hat{n}_0\hat{\vartheta}_0}, \tag{4.16a}$$

$$a_{GH} = -\frac{b^3\boldsymbol{\Omega}^2}{\hat{n}_0^{1/2}\hat{\vartheta}_0}, \tag{4.16b}$$

$$a_{HG} = \frac{4\pi}{\hat{n}_0^{1/2}\hat{\vartheta}_0}, \tag{4.16c}$$

$$a_{HH} = -\frac{2}{x^2} - \frac{4\pi}{\hat{\vartheta}_0}, \tag{4.16d}$$

and with source term

$$S = \hat{E}_\omega^{(0)}\,\frac{x\hat{n}_0'}{\hat{n}_0^{1/2}}. \tag{4.17}$$

The form of (4.15) is convenient for numerical integration. We emphasize that (4.15) does not depend on the nuclear charge Ze. In the limit $T \to 0$, the equations take the same form, with the substitution

$$\lim_{T\to 0}\frac{8\pi}{\hat{\vartheta}_0} = 3\left(\tfrac{1}{2}\pi\hat{n}_0\right)^{1/3}. \tag{4.18}$$

We introduce the dimensionless plasma frequency $\boldsymbol{\Omega}_{p0}$ as

$$\boldsymbol{\Omega}_{p0} = \left(\frac{4\pi\hat{n}_0^{(0)}}{b^3}\right)^{1/2} = \frac{C^{3/4}}{b^{3/2}} = \frac{\hbar a_0}{Ze^2}\,\omega_{p0}, \tag{4.19}$$

and the variable $\hat{\alpha}$ as

$$\hat{\alpha} = \hat{\kappa}\left(1 - \frac{\boldsymbol{\Omega}^2}{\boldsymbol{\Omega}_{p0}^2}\right)^{1/2}, \tag{4.20}$$

with the negative imaginary root chosen for $\boldsymbol{\Omega}^2 > \boldsymbol{\Omega}_{p0}^2$. For $\boldsymbol{\Omega} > \boldsymbol{\Omega}_{p0}$, the solution

of (4.15) corresponds asymptotically to outgoing plasma waves of the form

$$G(x) \sim -\frac{b^3\Omega^2}{\hat{\alpha}^2(\hat{n}_0^{(0)})^{1/2}}\, Q_\omega\, x k_1(\hat{\alpha}x) + \hat{p}_\omega^{(1)}\, \frac{(\hat{n}_0^{(0)})^{1/2}}{x}, \tag{4.21a}$$

$$H(x) \sim -\frac{4\pi Q_\omega}{\hat{\alpha}^2}\, x k_1(\hat{\alpha}x) + \frac{\hat{p}_\omega^{(1)}}{x} \quad \text{as} \quad x \to \infty, \tag{4.21b}$$

where $k_1(z) = e^{-z}(1+z)/z^2$ is a modified spherical Bessel function, and with coefficients Q_ω and $\hat{p}_\omega^{(1)}$ to be determined from the behaviour of $G(x)$ and $H(x)$ for small x. From (4.13), we find for the asymptotic behaviour of the function $K(x)$

$$K(x) \sim Q_\omega\, x k_1(\hat{\alpha}x) \quad \text{as} \quad x \to \infty. \tag{4.22}$$

For $0 < \Omega < \Omega_{p0}$, the solutions have the same asymptotic form, but then the function $k_1(\hat{\alpha}x)$ is exponentially damped, and the dipolar terms proportional to $\hat{p}_\omega^{(1)}$ dominate, as shown already in (4.10).

From (4.15), one finds for the behaviour of the functions $G(x)$ and $H(x)$ for small x

$$G(x) \sim \frac{\hat{E}_\omega^{(0)}}{2\pi^{1/2}}\, x^{5/4} + C_1 x^{1/2+\sqrt{33}/4} \quad \text{as} \quad x \to 0, \tag{4.23a}$$

$$H(x) \sim C_2\, x^2 \quad \text{as} \quad x \to 0, \tag{4.23b}$$

with as-yet unknown coefficients C_1 and C_2, which must be adjusted such as to recover the asymptotic behaviour shown in (4.21). It is convenient to consider the pair of functions $H(x), K(x)$ instead of $G(x), H(x)$, since in the asymptotic behaviour of the function $K(x)$ the dipolar terms cancel. If the differential equations (4.15) are solved with initial behaviour as shown in (4.23) with chosen values $C_{1\gamma}$ and $C_{2\gamma}$ then the asymptotic behaviour of the functions $H_\gamma(x)$ and $K_\gamma(x)$ is

$$K_\gamma(x) \sim P_{K\gamma} x\, i_1(\hat{\alpha}x) + Q_{K\gamma} x k_1(\hat{\alpha}x) \quad \text{as} \quad x \to \infty \tag{4.24a}$$

$$H_\gamma(x) \sim -\frac{4\pi}{\hat{\alpha}^2}\, K_\gamma(x) + P_{H\gamma} x^2 + \frac{Q_{H\gamma}}{x} \quad \text{as} \quad x \to \infty \tag{4.24b}$$

with certain coefficients $P_{K\gamma}$, $Q_{K\gamma}$, $P_{H\gamma}$ and $Q_{H\gamma}$. If we choose three trial pairs of values $(C_{1\gamma}, C_{2\gamma})$ then we obtain three pairs of functions $(K_\gamma(x), H_\gamma(x))$, and can construct a linear combination

$$K(x) = \sum_{\gamma=1}^{3} a_\gamma\, K_\gamma(x), \tag{4.25a}$$

$$H(x) = \sum_{\gamma=1}^{3} a_\gamma\, H_\gamma(x), \tag{4.25b}$$

with coefficients a_1, a_2 and a_3 satisfying

$$a_1 + a_2 + a_3 = 1, \tag{4.26a}$$

$$\sum_{\gamma=1}^{3} a_\gamma\, P_{K\gamma} = 0, \tag{4.26b}$$

$$\sum_{\gamma=1}^{3} a_\gamma\, P_{H\gamma} = 0. \tag{4.26c}$$

The coefficients ($P_{K\gamma}$, $Q_{K\gamma}$, $P_{H\gamma}$, $Q_{H\gamma}$) are found from the values of the solutions $K_\gamma(x)$ and $H_\gamma(x)$ at a pair of large distances x_1, x_2. The coefficients a_1, a_2 and a_3 can be determined from the three equations (4.26). The desired value of the dipole moment follows from

$$\hat{p}_\omega^{(1)} = \sum_{\gamma=1}^{3} a_\gamma Q_{H\gamma}, \tag{4.27}$$

and the value of the coefficient Q_ω can be found similarly. One can improve the numerical accuracy of the result by repeating the calculation with the found values C_1 and C_2 as one of the trial pairs. The procedure can be repeated several times until the coefficient $\hat{p}_\omega^{(1)}$ does not change appreciably.

By comparison of (4.10), (4.11) and (4.19), it follows that the magnitude of the dipole moment $\mathbf{p}_\omega^{(1)}$ is

$$p_\omega^{(1)} = Zea\hat{p}_\omega^{(1)}, \tag{4.28}$$

with ion radius

$$a = Z^{-1/3} b a_0. \tag{4.29}$$

The single-ion polarizability $\alpha_1'(\omega)$ is defined from the relation (Felderhof *et al.* 1995a).

$$p_\omega^{(1)} = \alpha_1'(\omega) E_\omega^{(0)}. \tag{4.30}$$

The corresponding dimensionless form is

$$\hat{p}_\omega^{(1)} = \hat{\alpha}_1'(\mathbf{\Omega}) \hat{E}_\omega^{(0)}. \tag{4.31}$$

By use of (4.14), one finds

$$\alpha_1'(\omega) = a^3 \hat{\alpha}_1'(\mathbf{\Omega}). \tag{4.32}$$

This relation allows one to cast the extinction cross-section in a scaling form.

5. Photoabsorption

In the electric dipole approximation, the cross-sections for absorption and scattering of radiation can be calculated from the electric dipole polarizability $\alpha_1'(\omega)$, defined in (4.30). The extinction cross-section is the sum of the cross-sections for absorption and scattering:

$$\sigma_{\rm ext}(\omega) = \sigma_{\rm abs}(\omega) + \sigma_{\rm sca}(\omega). \tag{5.1}$$

For the present model, the cross-sections vanish in the range $0 < \omega < \omega_{p0}$. The absorption for $\omega > \omega_{p0}$ is due to conversion of electromagnetic energy into longitudinal plasma waves. Previously a simple relation was derived between the cross-sections for absorption and scattering at the plasma frequency (Felderhof *et al.* 1995*b*):

$$\frac{\sigma_{\rm sca}(\omega_{p0}+)}{\sigma_{\rm ext}(\omega_{p0}+)} = 2\frac{s^3}{c^3}, \qquad s^2 = \frac{n_0^{(0)} \vartheta_0^{(0)}}{m}. \tag{5.2}$$

The ratio s/c usually is quite small, so that scattering can be neglected relative to absorption. In the following we consider only the extinction cross-section. It is given by (Felderhof *et al.* 1995*b*)

$$\sigma_{\rm ext}(\omega) = \frac{4\pi}{c} (\omega^2 - \omega_{p0}^2)^{1/2} \, {\rm Im}\, \alpha_1'(\omega). \tag{5.3}$$

By use of (4.13) and (4.32), this can be expressed as

$$\sigma_{\rm ext}(\omega) = \frac{4\pi e^2}{\hbar c} b^3 a_0^2 \, \hat{\sigma}_{\rm ext}(\mathbf{\Omega}), \tag{5.4}$$

with the dimensionless cross section

$$\hat{\sigma}_{\rm ext}(\mathbf{\Omega}) = (\mathbf{\Omega}^2 - \mathbf{\Omega}_{p0}^2)^{1/2} \, {\rm Im} \, \hat{\alpha}_1'(\mathbf{\Omega}). \tag{5.5}$$

Thus the cross-section $\sigma_{\rm ext}(\omega)$ takes a scaling form with frequency ω given by (4.13).

At the plasma frequency, the extinction cross-section $\hat{\sigma}_{\rm ext}(\mathbf{\Omega}_{p0}+)$ does not vanish, since the square root in (5.5) is cancelled by a corresponding singularity in Im $\hat{\alpha}_1'(\mathbf{\Omega})$. The limiting value is

$$\hat{\sigma}_{\rm ext}(\mathbf{\Omega}_{p0}+) = \hat{\beta}^{(1)} \mathbf{\Omega}_{p0} \tag{5.6}$$

with a coefficient $\hat{\beta}^{(1)}$ that can be found from the solution of (4.15) for frequency $\mathbf{\Omega}_{p0}$. At this particular frequency, the function $H(x)$ increases in proportion to x for large x. One can define the limiting slope

$$H_\infty = \lim_{x \to \infty} \frac{H(x)}{x} \qquad \text{at} \qquad \mathbf{\Omega} = \mathbf{\Omega}_{p0}. \tag{5.7}$$

The coefficient $\hat{\beta}^{(1)}$ in (5.6) is given by (Felderhof *et al.* 1995*b*)

$$\hat{\beta}^{(1)} = \frac{4}{3\hat{\kappa}} \, H_\infty^2. \tag{5.8}$$

For high frequency $\mathbf{\Omega}$, the reduced cross-section $\hat{\sigma}_{\rm ext}(\mathbf{\Omega})$ shows universal behaviour, and becomes independent of asymptotic electron density $\hat{n}_0^{(0)}$ and reduced temperature $\hat{T}$. The behaviour is identical to that found by Ball *et al.* (1973) for the atom in vacuum:

$$\hat{\sigma}_{\rm ext}(\mathbf{\Omega}) \sim \frac{1024}{81\sqrt{3}} \, \frac{K_\nu^2}{\pi^2} \, \frac{1}{\mathbf{\Omega}^2} = \frac{0.70144}{\mathbf{\Omega}^2} \qquad \text{as} \qquad \mathbf{\Omega} \to \infty, \tag{5.9}$$

with coefficient

$$K_\nu = \int_0^\infty z^{-1/2} J_\nu(z) \, dz, \qquad \nu = \frac{\sqrt{33}}{6}, \tag{5.10}$$

where $J_\nu(z)$ is the Bessel function of fractional order ν. The numerical value for the integral is $K_\nu = 0.973\,91$. At high frequency, the absorption is due to emission of plasma waves by electrons close to the nucleus, where the reduced density $\hat{n}_0(x)$ has the universal behaviour shown in (3.2). A more detailed explanation of the high-frequency behaviour shown in (5.9) will be presented elsewhere (Ishikawa and Felderhof 1998*b*).

The intermediate behaviour of the cross-section $\hat{\sigma}_{\rm ext}(\mathbf{\Omega})$ is characterized by a single broad resonance, dependent on asymptotic electron density and on temperature. A rough description of the resonance involves two sum rules, which follow from the theory for a general equilibrium profile. The first sum rule reads (Felderhof *et al.* 1995*b*)

$$R_T \equiv \int_{\mathbf{\Omega}_{p0}}^\infty \frac{\mathbf{\Omega}}{(\mathbf{\Omega}^2 - \mathbf{\Omega}_{p0}^2)^{1/2}} \hat{\sigma}_{\rm ext}(\mathbf{\Omega}) \, d\mathbf{\Omega} = \tfrac{1}{2}\pi (g_0 - \hat{\beta}^{(0)}) \mathbf{\Omega}_{p0}^2, \tag{5.11}$$

where the coefficient g_0 is found from equation (3.14) of Felderhof *et al.* (1995*b*) as

$$g_0 = \frac{1}{4\pi \hat{n}_0^{(0)}}, \tag{5.12}$$

and the coefficient $\hat{\beta}^{(0)}$ is given by equation (6.29) of Felderhof *et al.* (1995*b*) as

$$\hat{\beta}^{(0)} = \frac{2}{\hat{\kappa}^2} H_\infty. \tag{5.13}$$

The second sum rule reads (Felderhof *et al.* 1995*b*)

$$\int_{\Omega_{p0}}^{\infty} \frac{1}{\Omega(\Omega^2 - \Omega_{p0}^2)^{1/2}} \hat{\sigma}_{\rm ext}(\boldsymbol{\Omega})\, d\boldsymbol{\Omega} = \tfrac{1}{2}\pi(g_1 - \hat{\beta}^{(0)}), \tag{5.14}$$

where the coefficient g_1 is identical with the polarizability at zero frequency,

$$g_1 = \hat{\alpha}_1'(0), \tag{5.15}$$

as follows from equation (3.9) in Felderhof *et al.* (1995*b*) (note that in equation (7.16) of that paper the factor $\frac{1}{2}\pi$ should be deleted). Thus, in order to implement the sum rules, we need the solution of (4.15) at the two special frequencies $\boldsymbol{\Omega} = 0$ and $\boldsymbol{\Omega} = \boldsymbol{\Omega}_{p0}$. A mean absorption frequency may be defined as

$$\boldsymbol{\Omega}_\sigma = \left(\frac{g_0 - \hat{\beta}^{(0)}}{g_1 - \hat{\beta}^{(0)}}\right)^{1/2} \boldsymbol{\Omega}_{p0}. \tag{5.16}$$

We have checked the sum rules for several cases by comparison with the complete solution at all frequencies, and found good agreement.

The integral in (5.11) may be regarded as a measure of the integrated cross-section. In Fig. 7 we plot its value as a function of dimensionless temperature for various values of the asymptotic density $\hat{n}_0^{(0)}$. For low density and temperature, one finds agreement with the value of Ball *et al.* (1973):

$$\int_0^{\infty} \hat{\sigma}_{\rm ext}(\boldsymbol{\Omega})\, d\boldsymbol{\Omega} = \frac{64}{9\pi} = 2.2635 \qquad (\hat{n}_0^{(0)} = 0, \hat{T} = 0), \tag{5.17}$$

corresponding to $\hat{\beta}^{(0)}\Omega_{p0}^2 = 0$ in this limit. In Fig. 8 we plot the limiting value $\hat{\sigma}_{\rm ext}(\boldsymbol{\Omega}_{p0}+) = \hat{\beta}^{(1)}\boldsymbol{\Omega}_{p0}$ as a function of temperature $\hat{T}$ for various densities $\hat{n}_0^{(0)}$. Ball *et al.* (1973) found for the limiting value

$$\hat{\sigma}_{\rm ext}(\boldsymbol{\Omega}_{p0}+) = \tfrac{32}{9}\sqrt{3}\,(4.36)^2 = 117.1 \qquad (\hat{n}_0^{(0)} = 0, \hat{T} = 0). \tag{5.18}$$

In Fig. 9 we plot the ratio $\boldsymbol{\Omega}_\sigma/\boldsymbol{\Omega}_{p0}$, as given by (5.16), as a function of temperature $\hat{T}$ for various densities $\hat{n}_0^{(0)}$.

The results of our analysis are strikingly summarized in Fig. 7. This shows that the integrated extinction cross-section depends strongly on both the asymptotic electron density $n_0^{(0)}$ and the temperature T. The effect of temperature is the most dramatic. For fixed ion density, the integrated cross-section drops by orders of magnitude as the temperature increases. At the same time, the dependence on frequency changes, as indicated by Figs 8 and 9.

6. Approximate description

The numerical solution of (4.15) allows one to calculate the frequency-dependent extinction cross-section of an ion immersed in a plasma, within the framework of Bloch's hydrodynamic model. We have chosen a particular form for the equilibrium electron density profile of the ion, but other forms could be treated with the same amount of effort. The scheme requires a separate solution for each frequency,

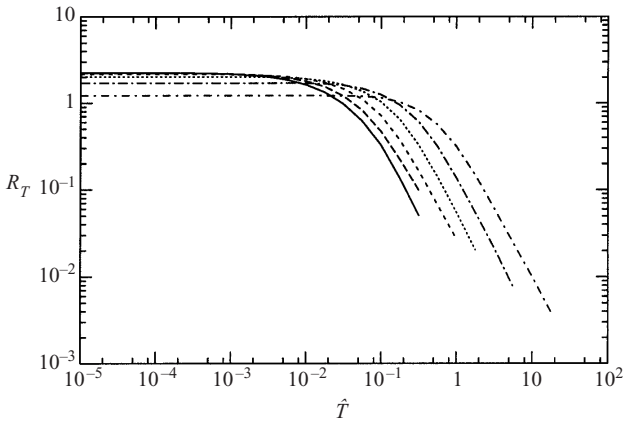

Figure 7. Integrated cross-section R_T, as defined by (5.11), as a function of reduced temperature $\hat{T}$ for density $\hat{n}_0^{(0)} = 10^{-7}$ (solid line), 10^{-6} (long dashes), 10^{-5} (short dashes), 10^{-4} (dotted line), 10^{-3} (long dashes, dots), 10^{-2} (short dashes, dots).

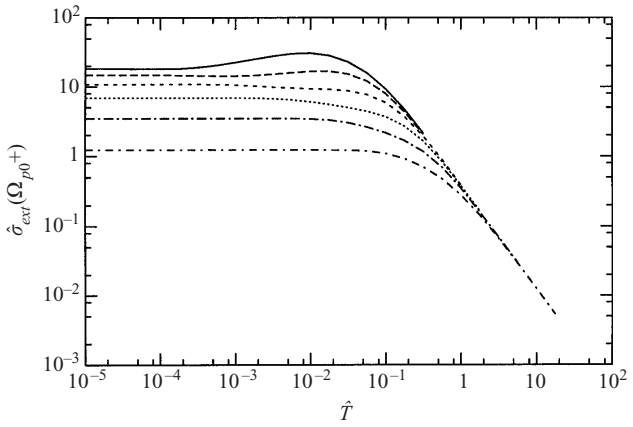

Figure 8. Reduced cross-section $\hat{\sigma}_{\rm ext}(\Omega_{p0}+)$ at the plasma frequency Ω_{p0} as a function of reduced temperature $\hat{T}$ for various densities $\hat{n}_0^{(0)}$, as in Fig. 7.

and therefore is fairly time-consuming. It is worthwhile to look for an approximate description, involving only a limited number of parameters and accounting for the main features of the absorption spectrum. Padé approximants provide the necessary tool.

As shown in previous work (Felderhof *et al.* 1995*b*, *c*), the exact polarizability $\hat{\alpha}_1'(\Omega)$ can be cast in the form

$$\hat{\alpha}_1'(\Omega) = \frac{1}{\Omega^2 - \Omega_{p0}^2} \, [A\Omega^2\Gamma(y) - g_1\Omega_{p0}^2] \tag{6.1}$$

with the coefficient A given by

$$A = g_1 - \hat{\beta}^{(0)} \tag{6.2}$$

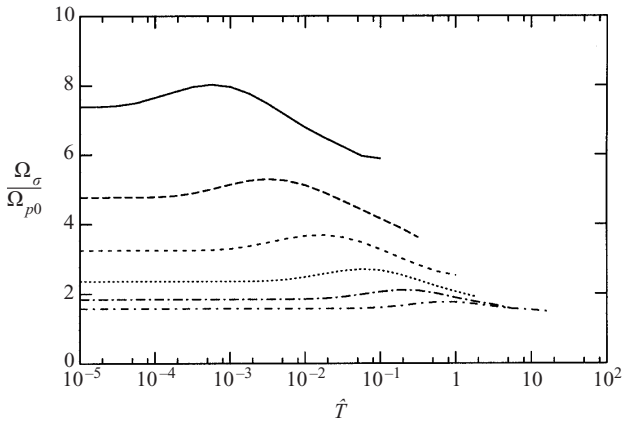

Figure 9. The ratio $\Omega_\sigma/\Omega_{p0}$, as given by (5.16), as a function of reduced temperature $\hat{T}$ for various densities $\hat{n}_0^{(0)}$, as in Fig. 7.

and the complex variable y defined by

$$y = \frac{1}{M}\left(1 - \frac{\Omega^2}{\Omega_{p0}^2}\right)^{1/2} \tag{6.3}$$

with the negative imaginary root chosen for $\Omega^2 > \Omega_{p0}^2$ and with coefficient

$$M = \left(\frac{g_0 - g_1}{A}\right)^{1/2}. \tag{6.4}$$

The function $\Gamma(y)$ is required to have the behaviour

$$\Gamma(0) = 1, \qquad \Gamma(y) \sim \frac{1}{y^2} \qquad \text{as} \qquad y \to \infty. \tag{6.5}$$

These conditions guarantee that the sum rules (5.11) and (5.14) are satisfied. Furthermore, the behaviour near the plasma frequency is described by

$$\Gamma(y) = 1 - Qy + O(y^2) \tag{6.6}$$

for small y, with coefficient

$$Q = M\,\hat{\beta}^{(1)}/A. \tag{6.7}$$

The high-frequency behaviour given by (5.9) shows that the function $\Gamma(y)$ has the asymptotic expansion

$$\Gamma(y) = \frac{1}{y^2} + \frac{D}{y^3} + O(y^{-4}), \tag{6.8}$$

with coefficient

$$D = -\frac{1024}{81\sqrt{3}\pi^2}\,\frac{K_\nu^2}{AM^3\Omega_{p0}^3}. \tag{6.9}$$

The approximate expression

$$\Gamma_E(y) = \frac{1}{1 + Qy + y^2 + \dfrac{y^2}{1 + Ey}}, \tag{6.10}$$

with coefficient

$$E = \frac{-1}{Q + D}, \tag{6.11}$$

has the properties shown in (6.6) and (6.8). The extrapolation function $\Gamma_E(y)$ has three poles in the complex y plane. In order to determine the polarizability $\hat{\alpha}_1'(\boldsymbol{\Omega})$ in the form (6.1) with approximate function $\Gamma_E(y)$, only the solution of (4.17) for $\boldsymbol{\Omega} = 0$ and $\boldsymbol{\Omega} = \boldsymbol{\Omega}_{p0}$ is required.

We can improve the approximation by including a larger number of poles. The improved approximation is constructed conveniently by the method of N-point Padé approximants. Thus, instead of (6.10), we write

$$\Gamma_{p+1}(y) = \frac{1}{1 + Qy + y^2 + y^2\,\psi_p(y)}, \tag{6.12}$$

where $\psi_p(y)$ is a ratio of two polynomials. The coefficients in the polynomials can be determined from known values of the function $\Gamma(y)$ at $p + 1$ points on the positive y axis. Elsewhere, two of us have discussed the method in detail (Cichocki and Felderhof 1994). It follows from (6.3) that positive y corresponds to pure imaginary frequency $\boldsymbol{\Omega}$. For such values, $\hat{\alpha}$ in (4.20) is positive, and the function $k_1(\hat{\alpha}x)$ in (4.21) decays exponentially. This implies that the asymptotic behaviour of the functions $G(x)$ and $H(x)$ is no longer described by (4.21) if $\hat{\alpha}$ is larger than $\hat{\kappa}$, since then the spatial variation of the profiles $\hat{n}_0(x)$ and $\hat{\vartheta}_0(x)$ must be taken into account. This can be done with some effort, and accurate values for the dipole moment can again be determined. Besides the solution of (4.15) for $\boldsymbol{\Omega} = 0$ and $\boldsymbol{\Omega} = \boldsymbol{\Omega}_{p0}$ one needs the solution for $p + 1$ positive imaginary frequencies. We have found that even more rapid convergence is obtained by using $p + 1$ points on the negative imaginary y axis, corresponding to $p + 1$ real frequencies. At the same time, one uses the $p + 1$ conjugate points on the positive imaginary y axis and the corresponding complex-conjugate values of the function $\Gamma(y)$. We have employed this method in our explicit calculations.

In the following we show plots of the cross-section $\hat{\sigma}_{\mathrm{ext}}(\boldsymbol{\Omega})$ as a function of $\boldsymbol{\Omega}$ for various values of number density $\hat{n}_0^{(0)}$ and temperature $\hat{T}$, as calculated from the numerical solution of (4.15), as calculated from (6.1) with the approximation $\Gamma_E(y)$, as given by (6.10) for the function $\Gamma(y)$, and as calculated with the Padé approximant (6.12). The calculations show that the approximation $\Gamma_E(y)$ is only qualitatively correct, and that accurate results require either the complete numerical solution of (4.15) at a dense set of frequencies or the solution by Padé approximants. The latter method is much faster than the former.

In Fig. 10 we plot the dimensionless cross-section $\hat{\sigma}_{\mathrm{ext}}(\boldsymbol{\Omega})$ as a function of frequency for reduced density $\hat{n}_0^{(0)} = 1.28 \times 10^{-6}$ and reduced temperature $\hat{T} = 0.008\,45$. This corresponds to 10% of solid density and a temperature of 20 eV for iron ($Z = 26$). In Fig. 11 we present similar plots for the same density $\hat{n}_0^{(0)} = 1.28 \times 10^{-6}$ and the higher temperature $\hat{T} = 0.0845$. In both cases the high-frequency asymptote $0.701\,44/\boldsymbol{\Omega}^2$ follows from (5.9). The results from the Padé approximant method cannot be distinguished from the exact ones on the scale of the figure.

In the Padé approximant method we have used the points

$$y_j = \frac{-i}{p - j + 1}\,\sqrt{500(j + 1)}, \qquad j = 0, \ldots, p \tag{6.13}$$

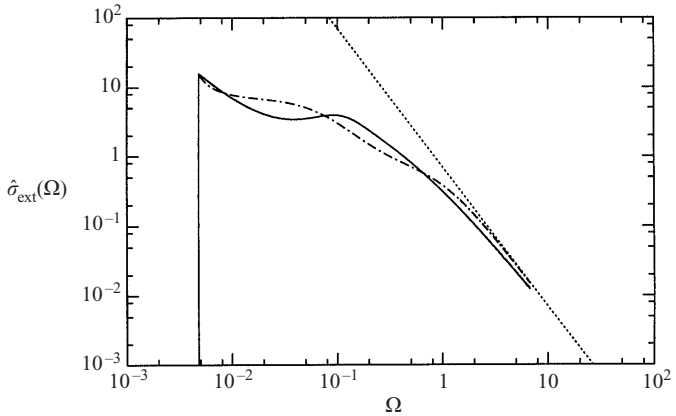

Figure 10. Reduced cross-section $\hat{\sigma}_{\rm ext}(\boldsymbol{\Omega})$ as a function of frequency $\boldsymbol{\Omega}$ for density $\hat{n}_0^{(0)} = 1.28 \times 10^{-6}$ and temperature $\hat{T} = 0.008\,45$, as calculated from the numerical solution of (4.15) (solid line), and as given by (5.5) and (6.1) with approximate function $\Gamma_E(y)$ given by (6.10) (dash-dotted line). The result of the Padé approximant method cannot be distinguished on the scale of the figure from the solid line. The curves tend to the universal asymptote $0.701\,44/\boldsymbol{\Omega}^2$ (dotted line).

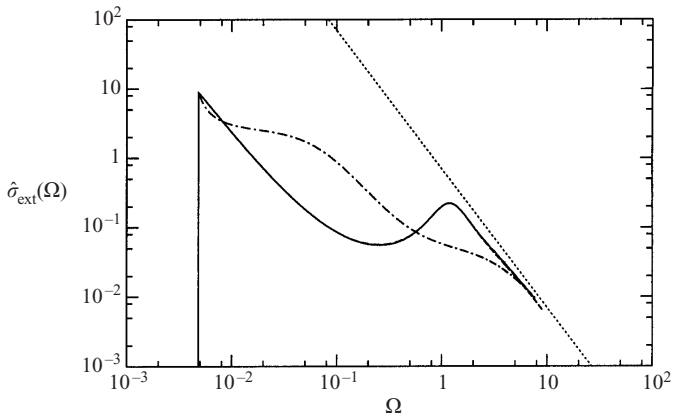

Figure 11. As in Fig. 10, but for density $\hat{n}_0^{(0)} = 1.28 \times 10^{-6}$ and temperature $\hat{T} = 0.0845$.

with $p = 7$ in Fig. 10 and $p = 9$ in Fig. 11. At the same time, the points $\{-y_j\}$ and corresponding values $\{\Gamma(-y_j) = \Gamma^*(y_j)\}$ are used. The range of points is chosen such as to cover a sufficiently wide range of frequencies. The values of the parameters A, M and Q for Fig. 10 are $A = 2056.6$, $M = 4.8957$ and $Q = 7.6549$. The corresponding values for Fig. 11 are $A = 958.23$, $M = 3.9844$ and $Q = 7.7003$.

Finally, we show in Fig. 12 the dimensionless cross-section $\hat{\sigma}_{\rm ext}(\boldsymbol{\Omega})$ at the low density $\hat{n}_0^{(0)} = 1.28 \times 10^{-6}$ for a range of temperatures, and compare with the numerical results of Ball *et al.* (1973) for the atom ($\hat{n}_0^{(0)} = 0$) at zero temperature. The decrease of the cross-section at intermediate frequencies with increasing temperature is due to ionization.

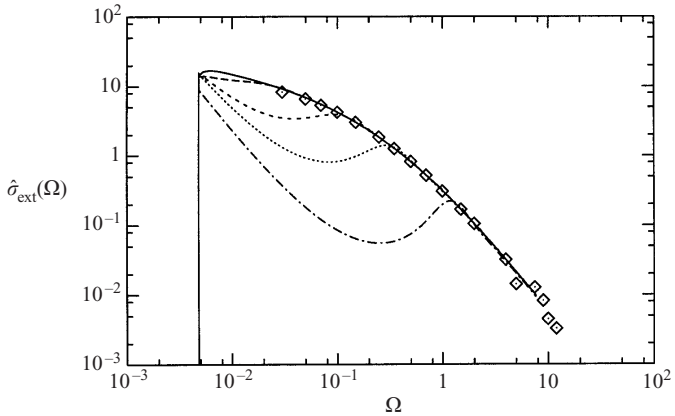

Figure 12. Reduced cross-section $\hat{\sigma}_{\rm ext}(\Omega)$ as a function of frequency Ω for density $\hat{n}_0^{(0)} = 1.28 \times 10^{-6}$ and temperature $\hat{T} = 0$ (solid line), 0.000 845 (long dashes), 0.008 45 (short dashes), 0.0267 (dotted line), 0.0845 (dash-dotted line). We compare with the numerical results of Ball *et al.* (1973) (diamonds).

7. Discussion

We have studied photoabsorption by an ion immersed in a plasma on the basis of an ion correlation model and the Thomas–Fermi approximation for the equilibrium electron distribution. The collective motion of the electron cloud is treated within the framework of Bloch's classical hydrodynamic model. Single-electron effects and quantum dynamics have been left out of consideration. The treatment provides a qualitative picture of the frequency-dependent photoabsorption cross-section. In the approximate model, the cross-section is found to scale with the nuclear charge. It also depends strongly on plasma density and temperature. To our knowledge, the present calculation is the first to yield a comprehensive picture of photoabsorption by an ion immersed in a plasma for any ion charge, density and temperature. We believe that the picture captures the gross features of the actual photoabsorption cross-section correctly, and regard it as a first step towards more elaborate and detailed calculations.

Our numerical results for the degree of ionization, the equilibrium density profile and the photoabsorption cross-section are shown for several values of the reduced temperature $\hat{T}$ and the reduced asymptotic free-electron density $\hat{n}_0^{(0)}$. It may be useful to consider values of these reduced parameters relevant for future experiments in high-density plasmas. We choose two elements that have already been used in plasma transmission experiments (Winhart *et al.* 1995; Merdji *et al.* 1998): aluminium (Al, $Z = 13$) and samarium (Sm, $Z = 62$). The collective effects in photoabsorption on which we have focused our attention will be important in high-density plasmas. Large lasers of future generations will allow one to approach plasma densities of the order of solid density in X-ray transmission experiments in radiatively heated targets. In such plasmas the plasma frequency will range from about 15 eV to a few tens of eV. The corresponding reduced temperature $\hat{T}$ lies in the range 0.02–0.10 for Al and in the range 0.0026–0.013 for Sm. The reduced asymptotic density $\hat{n}_0^{(0)}$ corresponding to solid density will equal approximately $3.67 \times 10^{-5} Z_0$ (Al) for Al and $7.88 \times 10^{-7} Z_0$ (Sm) for Sm. We recall that the effective charge number $Z_0 = I_f Z$ depends on the degree of ionization I_f and hence

on temperature. The reduced density $\hat{n}_0^{(0)}$ may be found approximately from Figs 1 and 2, or more accurately from the self-consistent relation $Z_0 = I_f Z$. Finally, we note that our theoretical prediction for the photoabsorption cross section has been compared with recent experimental results (Theobald *et al.* 1998).

Acknowledgement

One of the authors (T. B.) acknowledges support from the Commissariat à l'Energie Atomique, Centre d'Etudes Limeil-Valenton.

References

Abdallah Jr, J. and Clark, R. E. H. 1991 X-ray transmission calculations for an aluminum plasma. *J. Appl. Phys.* **69**, 23–26.

Antia, H. M. 1993 Rational function approximations for Fermi-Dirac integrals. *Astrophys. J. Suppl.* **84**, 101–108.

Armstrong, B. H. and Nicholls, R. W. 1972 *Emission, Absorption and Transfer of Radiation in Heated Atmospheres*. Pergamon, Oxford.

Ball, J. A., Wheeler, J. A. and Firemen, E. L. 1973 Photoabsorption and charge oscillation of the Thomas–Fermi atom. *Rev. Mod. Phys.* **45**, 333–352.

Bar-Shalom, A., Oreg, J., Goldstein, W. H., Shvarts, D. and Zigler, A. 1989 Super-transition-arrays: a model for the spectral analysis of hot, dense plasma. *Phys. Rev.* **A40**, 3183–3193.

Blenski, T. and Cichocki, B. 1992 Linear response of partially ionized, dense plasma. *Laser Particle Beams*, **10**, 299–309.

Blenski, T. and Cichocki, B. 1994 Polarizability of partially ionized dense plasmas (application to photo-absorption calculations). *J. Quant. Spectrosc. Radiat. Transfer* **51**, 49–58.

Blenski, T., Grimaldi, A. and Perrot, F. 1997 Hartree–Fock statistical approach to atoms and photoabsorption in plasma. *Phys. Rev.* **E55**, 4889–4892.

Bloch, F. 1933 Bremsvermögen von Atomen mit mehreren Elektronen. *Z. Phys.* **81**, 363–376.

Cauble, R., Blaha, M. and Davis, J. 1984 Comparison of atomic potentials and eigenvalues in strongly coupled neon plasma. *Phys. Rev.* **A29**, 3280–3287.

Cichocki, B. and Felderhof, B. U. 1994 Slow dynamics of linear relaxation systems. *Physica* **A211**, 165–192.

Cody, W. J. and Thacher, H. C., 1967 Rational Chebyshew approximations for Fermi–Dirac integrals of orders $-\frac{1}{2}$, $\frac{1}{2}$ and $\frac{3}{2}$. *Math. Comput.* **21**, 30–40.

Crowley, B. J. B. 1990 Average-atom quantum-statistical cell model for hot plasma in local thermodynamic equilibrium over a wide range of densities. *Phys. Rev.* **A41**, 2179.

Da Silva, L. B., MacGowan, B. J., Kania, D. R., Hammel, B. A., Back, C. A., Hsieh, E., Doyas, R., Iglesias, C. A., Rogers, F. J. and Lee, R. W., 1992 Absorption measurements demonstrating the importance of $\Delta n = 0$ transitions in the opacity of iron. *Phys. Rev. Lett.* **69**, 438–441.

Davidson S. J., Foster, J. M., Smith, C. C., Warburton, K. A. and Rose, S. J. 1988 Investigation of the opacity of hot, dense aluminum in the region of its K edge. *Appl. Phys. Lett.* **71**, 847–849.

Englert, B.-G., 1988 *Semiclassical Theory of Atoms*. Lecture Notes in Physics, Vol. 300. Springer-Verlag, Berlin.

Felderhof, B.U., Blenski, T. and Cichocki, B. 1995*a* Dielectric function of an electron-ion plasma in the optical and X-ray regime. *Physica* **A217**, 161–174.

Felderhof, B. U., Blenski, T. and Cichocki, B. 1995*b* Collective contribution to the frequency-dependent polarizability of an ion or metallic cluster immersed in a plasma. *Physica* **A217**, 175–195.

Felderhof, B. U., Blenski, T. and Cichocki, B. 1995*c* Frequency-dependent extinction cross section of a spherical ion or metallic cluster immersed in a plasma. *Physica* **A217**, 196–213.

Foster, J. M., Hoarty, D. J., Smith, C. C., Rosen, P. A., Davidson, S. J., Rose, S. J., Perry, T. S. and Serduke F. J. D. 1991 L-shell absorption spectrum of an open M-shell germanium plasma: comparison of experimental data with a detailed configuration-accounting calculation. *Phys. Rev. Lett.* **67**, 3255–3258.

Goldberg, A., Rozsnyai, B. F. and Thompson, P. 1986 Intermediate-coupling calculation of atomic spectra from hot plasma. *Phys. Rev.* **A34**, 421–427.

Grimaldi, F., Grimaldi-Lecourt, A. and Dharma-wardana, M. W. C. 1985 Time-dependent density-functional theory of light absorption in dense plasmas: application to iron plasma. *Phys. Rev.* **A32**, 1063–1071.

Ishikawa, K. and Felderhof, B. U. 1998*a* Dielectric response in Bloch's hydrodynamic model of an electron-ion plasma. *Physica* **A250**, 506–516.

Ishikawa, K. and Felderhof, B. U. 1998*b* High-frequency photoabsorption by an ion immersed in a plasma at any temperature. *Physica* **A253**, 541–554.

Keady, J. J., Abdallah, J. A. and Clark, R. E. H. 1993 Accurate methods for calculating atomic processes in high-temperature plasmas. *Proceedings of 14th International Conference on Plasma Physics and Controlled Nuclear Fusion Research*, Vol. 3, pp. 205–208. IAEA, Vienna.

Landau, L. D. and Lifshitz, E. M. 1965 *Quantum Mechanics*, pp. 241–246. Pergamon, Oxford.

Landau, L. D. and Lifshitz, E. M. 1968 *Statistical Physics*, p. 155. Pergamon, Oxford.

Lee, R. W., Petrasco, R. and Falcone, R. W. 1995 Science on high-energy lasers: from today to the NIF. *LLNL Report* UCRL-ID-119170.

Mahan, G. D. and Subbaswamy, K. R. 1990 Local Density Theory of Polarizability. Plenum, New York.

Mayer, H. 1949 Methods of opacity calculations. *Report* LA-647.

Merdji, H., Mißalla, T., Blenski, T., Perrot, F., Gauthier, J. C., Eidmann, K. and Chenais-Popovics, C. 1958 Absorption spectroscopy of a radiatively heated samarium plasma. *Phys. Rev.* **E57**, 1042–1046.

Perrot, F. and Dharma-wardana, M. W. C. 1993 Photoabsorption K edge of shock compressed aluminum. *Phys. Rev. Lett.* **71**, 797–800.

Perrot, F. 1982 Temperature-dependent screening of neon in an electron gas. Application to pair-potential calculations. *Phys. Rev.* **A26**, 1035–1041.

Perry, T. S., Davidson, S. J. and Serduke F. J. D. 1991 Opacity measurements in a hot dense medium. *Phys. Rev. Lett.* **67**, 3784–3787.

Rogers, F. J. and Iglesias, C. A. 1992 Radiative atomic Rosseland mean opacity tables. *Astrophys. J. Suppl.* **79**, 507–568.

Sturm, K., Zaremba, E. and Nuroh, K. 1990 Core polarization and the dielectric response of simple metals. *Phys. Rev.* **B42**, 6973–6992.

Theobald, W., Häßner, R., Sauerbrey, R., Fehr, R., Gericke, O., Schlanges, M., Kraeft, W.-D. and Ishikawa, K. 1998 Dielectric function of femtosecond laser-produced plasmas. Preprint.

Winhart, G., Eidmann, K., Iglesias, C. A., Bar-Shalom, A., Minguez, E., Rickert, A. and Rose, S. 1995 XUV opacity measurements and comparison with models. *J. Quant. Spectrosc. Radiat. Transfer* **54**, 437–446.

Zangwill, A. and Liberman, D. A. 1984 On the interplay between dielectric screening and core hole relaxation in soft X-ray absorption. *J. Phys.* **B17**, 253–257.

Zangwill, A. and Soven, P. 1980 Density-functional approach to local-field effects in finite systems: photoabsorption in the rare gases. *Phys. Rev.* **A21**, 1561–1572.

Zaremba, E. and Sturm, K. 1991 Soft-X-ray absorption spectra and corethreshold behavior in the alkali metals. *Phys. Rev. Lett.* **66**, 2144–2147.